HAL
open science

A Viewpoint on Hot Spots in Microwave Sintering and Flash Sintering

Jean-Marc Chaix, Renaud Bouchet, Didier Bouvard, Timothée Fabre, Tristan Garnault, Christelle Harnois, Kouami Koutoati, Marie Lachal, Sylvain Marinel, Marlu Cesar Steil

To cite this version:

Jean-Marc Chaix, Renaud Bouchet, Didier Bouvard, Timothée Fabre, Tristan Garnault, et al.. A Viewpoint on Hot Spots in Microwave Sintering and Flash Sintering. Advanced Engineering Materials, 2023, 25 (18), 10.1002/adem.202201742 . hal-04287243

HAL Id: hal-04287243

https://cnrs.hal.science/hal-04287243

Submitted on 15 Nov 2023

HAL is a multi-disciplinary open access archive for the deposit and dissemination of scientific research documents, whether they are published or not. The documents may come from teaching and research institutions in France or abroad, or from public or private research centers.

L'archive ouverte pluridisciplinaire **HAL**, est destinée au dépôt et à la diffusion de documents scientifiques de niveau recherche, publiés ou non, émanant des établissements d'enseignement et de recherche français ou étrangers, des laboratoires publics ou privés.

A viewpoint on hot spots in microwave sintering and flash sintering

Jean-Marc Chaix[1], Renaud Bouchet[2], Didier Bouvard[1], Timothée Fabre[2], Tristan Garnault[1,3], Christelle Harnois[3], Kouami Koutoati[1], Marie Lachal[2], Sylvain Marinel[3], Marlu Cesar Steil[2]*

[1]Univ. Grenoble Alpes, CNRS, Grenoble INP, SIMaP, F-38000 Grenoble
[2]Univ. Grenoble Alpes, CNRS, Grenoble INP, LEPMI, F-38000 Grenoble
[3]Normandie Univ, CNRS, ENSICAEN, Lab CRISMAT, , F-14050 Caen, France

Abstract

Microwave sintering and flash sintering are field assisted ceramic processing techniques in which heating is totally or partly obtained inside the material itself by a coupling between the ceramic material and the electromagnetic or electrical field. They frequently give rise to the observation of localised temperature excess known as hot spots that can lead to dramatic effects on the sintered parts. This paper explores and discusses the common origin of hot spots in both techniques, their development and the possible ways for limiting their effects.

Keywords:

Flash sintering, microwave sintering, hot spots, ceramics

1. Introduction

Microwave sintering (MWS) [1]–[3] and Flash Sintering (FS) [4]–[6] are two techniques that involve the direct coupling between the ceramic powder parts to be heated and an electromagnetic or electrical power source. The effective heat source is therefore inside the bulk of the part and depends on the interaction of the constitutive matter with the electromagnetic field. These techniques are potentially energy efficient for sintering, as the heating a whole furnace up to the sintering temperature is not required, and they are expected to enable fast sintering, due to the limited thermal inertia of the parts. Both techniques however exhibit the problem of hot spots, *i.e.*, the development of local overheating in some regions of the part. It consists in a localization of coupling/heating and is promoted by the high heating rates. Specific additional "non-thermal" effects of the field on the sintering mechanisms and kinetics have been proposed and discussed in a number of papers, as well for FS [7][8] as for MWS [9]–[12], while other papers discuss the positive effect of the enabled high heating rates [13][14] but this discussion is out of the scope of the present paper. The purpose of the present paper is to discuss the common and specific aspects of the hot spot phenomenon in the two techniques and the ways that have been proposed to deal with this problem, in the light of literature data and new results.

2. FS and MWS techniques

2.1. *FS*

Since the early work by Cologna and Raj [15] who first described and named the Flash Sintering technique, FS is obtained by applying a DC or AC field to a ceramic powder compact preheated at a temperature much lower than its usual sintering temperature but high enough for ensuring a non-negligible electric conductivity[4]–[6]. Many papers deal with specimens with a dog-bone shape, well suited for direct observation and easy to setup, but classic cylindrical shapes are also used (**Figure 1**-a). The flash phenomenon is applied using a constant voltage V either when the temperature is stabilized at T_0 (isothermal experiments) or at the beginning of a temperature ramp (constant heating rate). In the first case, when suitable (high enough) T_0 and V are selected, a first period is observed in which the measured current through the specimen slowly increases (the so-called incubation period), before a dramatic increase in current suddenly occurs (Figure 1-b). This current surge is associated to a strong increase of temperature and a fast shrinkage of the specimen, easily observed in the case of dog-bone samples (see for instance videos by J Francis[16]). A flash of visible light emission is also observed. Although other interpretations have been proposed for the incubation time, sometimes with very sophisticated physical models [17], it is now admitted [18]–[22] that the thermal runaway induced by the Joule effect and the thermally activated electrical conductivity of the ceramics explains the coupled electrical and thermal surge as well as the flash in light. Indeed, if we consider a small thermally homogeneous and isolated sample submitted to a constant electric field E, the local Joule power density is

$$P = \sigma E^2 \tag{1}$$

where σ is the electrical conductivity and E the electric field, so that the temperature evolution is

$$\frac{\mathrm{d}T}{\mathrm{dt}} = \frac{\sigma E^2}{\rho \mathrm{C_p}} \tag{2}$$

where ρC_p is the volume heat capacity. When σ is thermally activated with an activation energy Q, this leads to a simple evolution equation:

$$\frac{dT}{dt} = \frac{\sigma_0 E^2}{\rho C_p} \exp\left(-\frac{Q}{RT}\right) \tag{3}$$

which can be easily numerically integrated (Figure 1-c) and clearly reproduces the experimental curves. This simple equation also explains the shorter "incubation time" for higher temperature T or higher electric field E. It however does not explain the experimentally observed threshold value for the occurrence of the flash phenomenon. This last observation requires to take into account the thermal losses term L, that depends on the specimen temperature T and the furnace temperature T_0 (typically terms in $(T - T_0)$ and $(T^4 - T_0^4)$) for conductive/convective and radiative exchanges, respectively). It comes:

$$\frac{dT}{dt} = \frac{\sigma_0 E^2}{\rho C_p} \exp\left(-\frac{Q}{RT}\right) - L(T, T_0) \tag{4}$$

The flash phenomenon is only observed when the heat source term exceeds the loss capacity [20][21][23], so that the thresholds in T or E correspond to a unique threshold in initial Joule power $\sigma(T_0)E^2$ [24].

Keeping the applied voltage constant when the flash occurs would lead to an infinite Joule power. In practice, in most experiments the power supply is switched to a constant intensity control, when the intensity reaches a predefined value I. The "classic" flash sintering technique therefore includes two steps, known as voltage control and current control stages, respectively (Figure 1-b). The intensity control step is generally maintained for several tenths of seconds, in order to improve the final density, as the densification during the short flash is significant but far from reaching full density. It is to be noticed that the switch intensity control, performed by an electronic device, is not instantaneous, so that uncontrolled overcurrent/overheating is unavoidable and systematic.

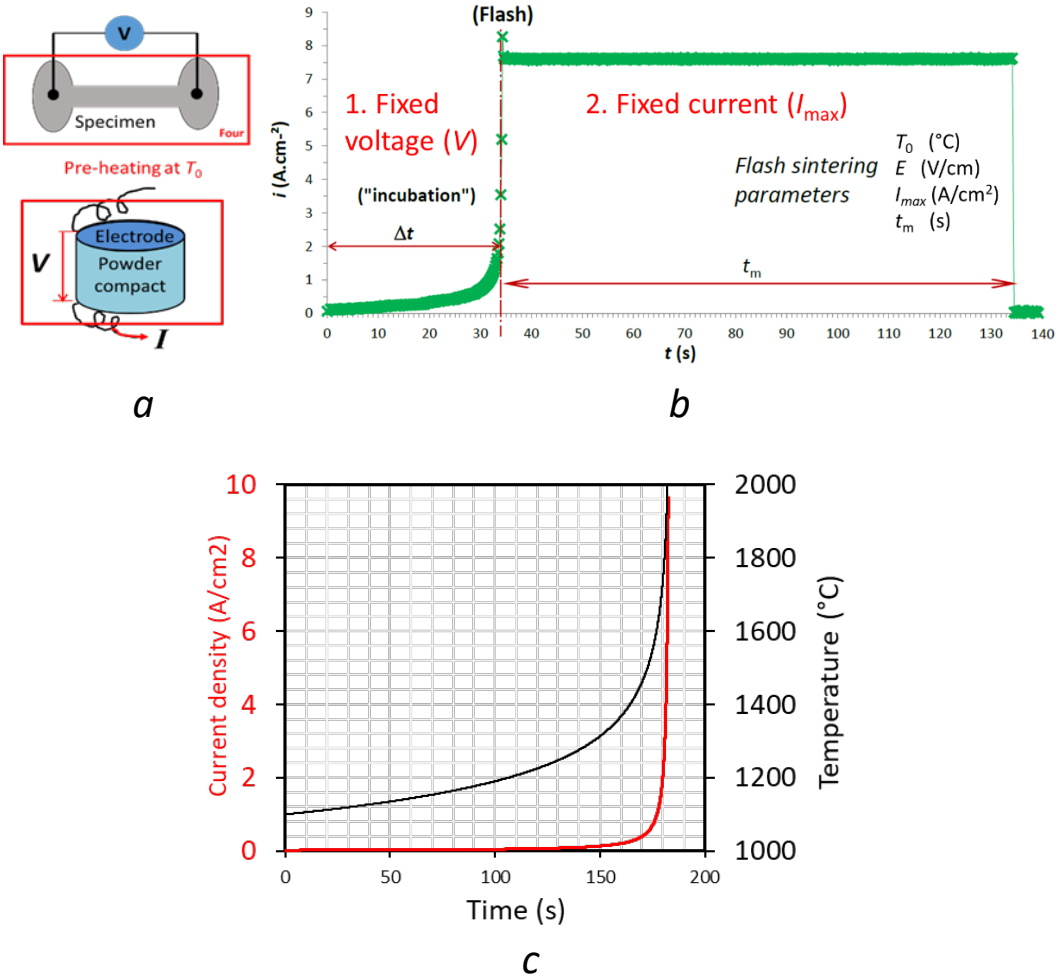

Figure 1. Flash sintering (FS): dog-bone and cylinder specimens (a); two steps experiments with fixed voltage V (fixed field E) before the flash event then fixed current I_{max} for time t_m (b) evolution of temperature and current during a FS experiment calculated from Equation 3 using data for 3YSZ from Todd et al.[18] (c).

2.2. *MW*

Microwave sintering [1]–[3] is operated in a microwave cavity, to which microwaves produced by a generator, generally a magnetron and more recently a solid state generator, are brought through a coaxial or rectangular waveguide. Two major types of cavities are used. The single mode cavity is the semi closed section of a waveguide, whose size can be adjusted to approach resonant conditions. In this case, the electric field distribution corresponds to stable stationary

waves (**Figure 2**-a) with defined high field nodes and antinodes. In such cavities, specimens with a size smaller than the half wavelength can be placed in almost constant electric fields areas. The second type of cavity, called multimode cavity, is a large one, generally a parallelepiped, in which multiple reflections of the waves on the sides lead to multiple propagation modes and to a complex and almost unpredictable distribution of the field (Figure 2-b). Several or large specimens can be placed at the same time in the multimode cavity; they are often placed on rotating plates in the purpose of obtaining a homogeneous time average of the field around it.

In this technique, the specimen can be directly heated by the interaction with the field, in most cases the electric field, the power density P being:

$$P = 2\pi f \varepsilon_0 \frac{\varepsilon_e'' E^2}{2} \quad (5)$$

where ε_0 is the dielectric permittivity, f the wave frequency and ε_e'' the imaginary part of the effective dielectric permittivity of the specimen. ε_e'' is often written $\varepsilon_e'' = \varepsilon_e' \tan\delta$, where ε_e' is the real part of the relative permittivity and $\tan\delta$ the so-called loss factor. In Equation 5, E is the electric field inside the material: it is in practice different from the externally applied field [3], but this point will not be discussed in the present paper.

In the case of microwave sintering, as high temperatures are required and the cavity walls are cold, the specimen is generally embedded in a thermally insulated box constituted by a highly porous fibrous or porous material, which is supposed to have low interaction with the field [3][25].

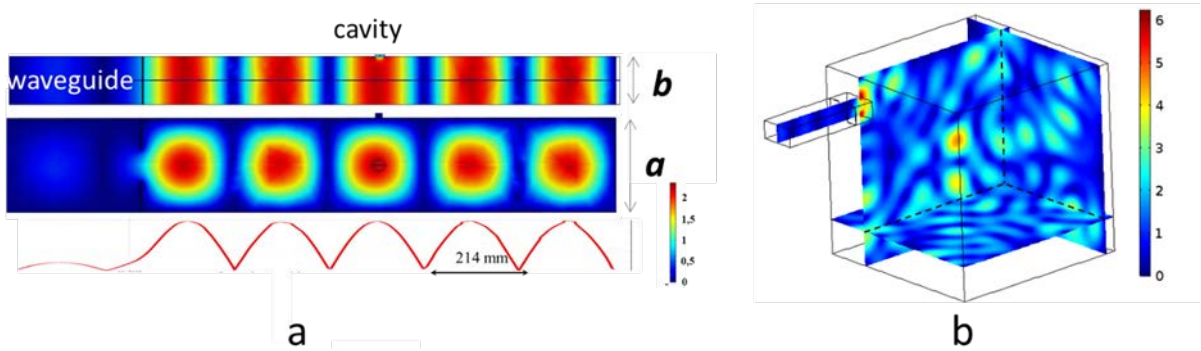

Figure 2. Geometry and electric field in the two major devices used in microwave sintering: single mode (a) and multimode(b) cavities.

A major point for the present paper is that the effective dielectric permittivity, which includes a contribution $\frac{\sigma}{2\pi f \varepsilon_0}$ of the electrical conductivity σ, strongly increases with increasing temperature, almost as a thermally activated property, in particular when this increase is due to the electrical conductivity [3][10]. This temperature dependency is an issue for the control of the heating rates during microwave sintering [26]–[28]. In the same way as in Joule heating, the microwave heating is therefore subject to thermal runaway phenomena, as demonstrated by Roussy *et al.* [29] using a simple model leading to practical criteria in the case of a second degree polynomial dependency of permittivity with temperature, or by Spotz *et al.*[30] in the case of alumina.

A direct link with FS was recently made by Bykov *et al.* [31] who suggested to use the thermal runaway in microwave heating to perform microwave flash sintering on the basis of an efficient control of the microwave input power.

3. Hot spots/localization of heating

3.1. *Basic instability*

The tendency to produce local overheating is a common feature to MWS and FS that reflects the intrinsic instability of the heating by direct coupling when the coupling parameter (ε_e'' or σ, respectively) increases with temperature. A similar equation defines the dissipated power density in both cases (Equation 1 and 5):

$$P \propto \gamma(T)\, E^2 \tag{6}$$

where the coupling property $\gamma(T)$ of the material has a positive temperature coefficient $\frac{d\gamma}{dT}$.

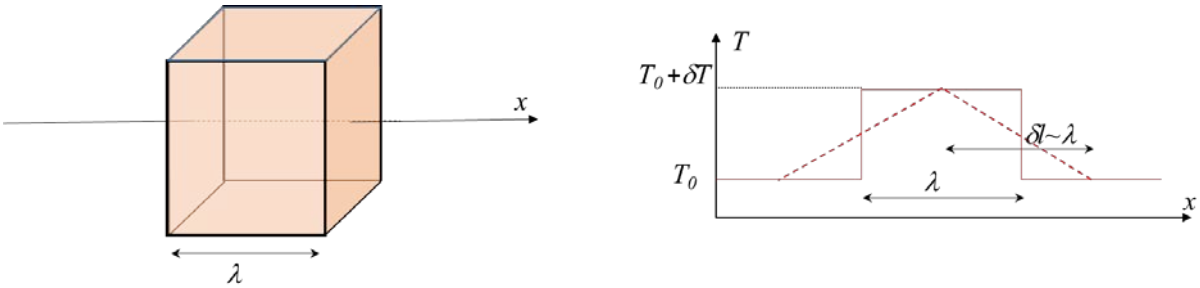

Figure 3. Small volume δV of length λ corresponding temperature profile (red line) and local approximate temperature gradient (red dotted line)

The instability can be understood using a simplified calculation. If we consider a small volume δV of the sample with a small perturbation of temperature δT with respect to its surroundings (**Figure 3**), this volume will exhibit a power excess δP with respect to its surroundings:

$$\delta P \propto \frac{d\gamma}{dT}\, E^2\, \delta T\, \delta V \tag{7}$$

while the outwards heat loss δL by heat diffusion (heat conductivity κ) along distance δl through the surface δS of the small volume is expected to dissipate this temperature excess:

$$\delta L \propto \kappa\, \frac{\delta T}{\delta l}\, \delta S \tag{8}$$

Where δl is the heat diffusion distance. The temperature perturbation will be damped when $(\delta P - \delta L) < 0$ and amplified if $(\delta P - \delta L) > 0$. In the case of positive temperature coefficient, $(\delta P - \delta L)$ can be positive and its sign is determined by the amplitude of the dimensionless power ratio

$$\frac{\delta P}{\delta L} \propto \frac{\frac{d\gamma}{dT}E^2}{\kappa}\frac{\delta V \delta l}{\delta S} \tag{9}$$

As both $\frac{\delta V}{\delta S}$ and δl scale with the size λ of the small volume, the dimensionless power to loss ratio Π can be written:

$$\Pi = \frac{\frac{d\gamma}{dT}E^2}{\kappa}\, \lambda^2 \tag{10}$$

Π determines the stability of the system. For large values of this ratio, any small over heating will be amplified, leading to heat localization and the formation of a hot spot. This oversimplified calculation helps understanding the conditions that favour the development of instabilities: high fields, *i.e.*, high power and high heating rates ; high positive temperature coefficients $\frac{d\gamma}{dT}$; low heat conductivity κ, *i.e.*, low heat dissipation. Equation 10 also means that the perturbation size λ must also be large enough, which of course requires that the sample itself is large enough. In any given processing conditions of a given material a large sample must systematically be unstable with respect to hot spots. These simple conclusions are valid for FS and MWS as well.

In the case of FS, Dong [32] proposed a more classic perturbation analysis of stability and obtained a critical size in the case of Joule heating in a 2D geometry (perpendicular to the E field axis), with thermally activated conductivity $\sigma = \sigma_0 \exp(-\frac{Q}{RT})$ (a typing error is present in equation 10 and 11 in Dong's original paper [32], where λ should be read λ^2; this error is reproduced in some citing papers).

$$\lambda_c = \left(\frac{2\kappa}{E^2 \sigma_0 \frac{Q}{RT_0^2} \exp(-\frac{Q}{RT_0})} \right)^{1/2} \tag{11}$$

that could be written, in the present notations:

$$\lambda_c = \left(\frac{2\kappa}{E^2 \frac{d\gamma}{dT}} \right)^{1/2} \tag{12}$$

This is typically equivalent to setting that the system is unstable when $\Pi > \Pi_c = 4$. Dong[32] estimated λ_c to typically 0.8-1.6 mm around 1000°C for YSZ, but it is to be noticed that in the case of thermally activated conductivity, $\frac{d\gamma}{dT}$ strongly increases with temperature, so that even smaller samples could be the seat of instabilities when temperature increases during FS. In the case of MW heating of alumina, Spotz *et al.* [30] also discussed a critical specimen size through the use of the Biot number. The intrinsically unstable character of microwave heating and the development of hot spots was also studied and discussed on the basis of computer simulations [33].

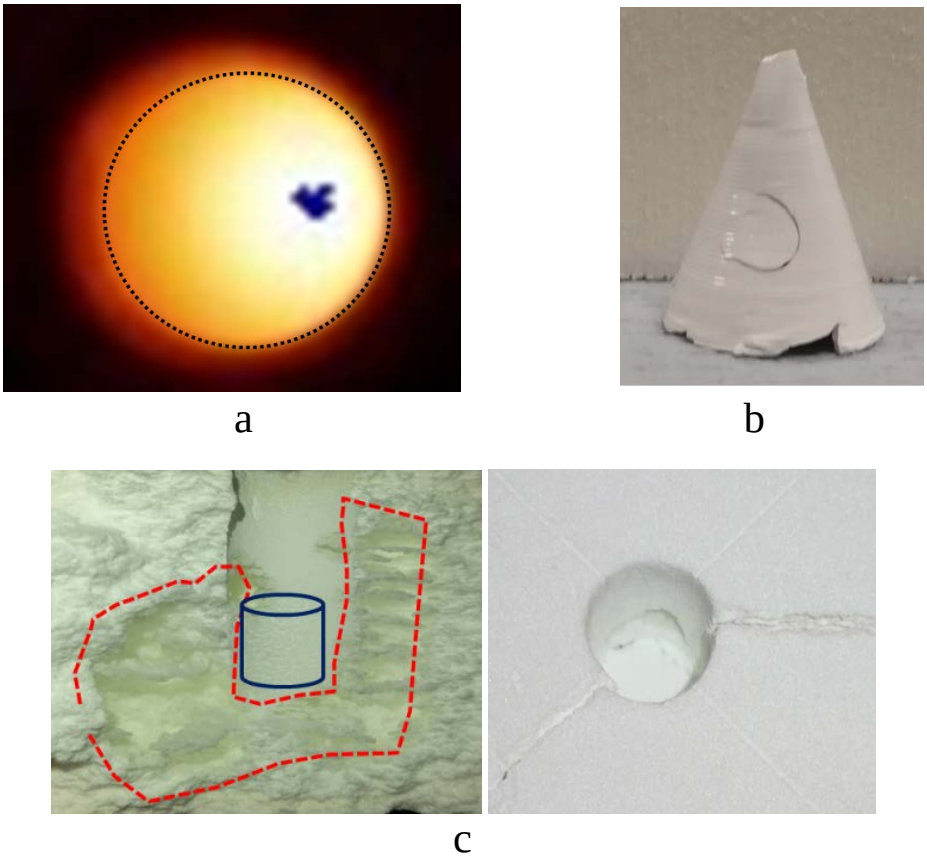

Figure 4. Hots spots during MWS: hot spot on the specimen surface observed by IR camera (a); local fracturing of a specimen during sintering due to local thermal stress stresses induced by hot spot (b); local melting of the thermal insulation around the specimen due to localised heating of the insulating material (c).[34]

3.2. *Development of the localisation*

In the case of microwave heating, the instability generally develops as a hot spot observed on the surface of the specimen (**Figure** 4-a) and the local overheating can lead to the fracture of the specimen (Figure 4-b) [28]. Hot spots can also develop inside the specimen, as shown in experiments as well as in numerical calculations [28][33]. They can also develop inside the insulating material placed around the specimen (Figure 4-c) in which the coupling with microwave is expected to be low but the very low thermal conductivity favours the development of hot spots [28].

In FS experiments, when the local thermal instability turns into localized thermal runaway, the localization develops along a preferential current path (high temperature = high conductivity) which results in a "hot line" rather than a hot spot [35][36]. The process therefore leads to strongly inhomogeneous samples (**Figure 5**): they are almost not densified but a region around a preferential current path that shows densification and grain growth, with sometimes melted zones [35][37], cavities [6] and even fractures or as-drilled holes [35].

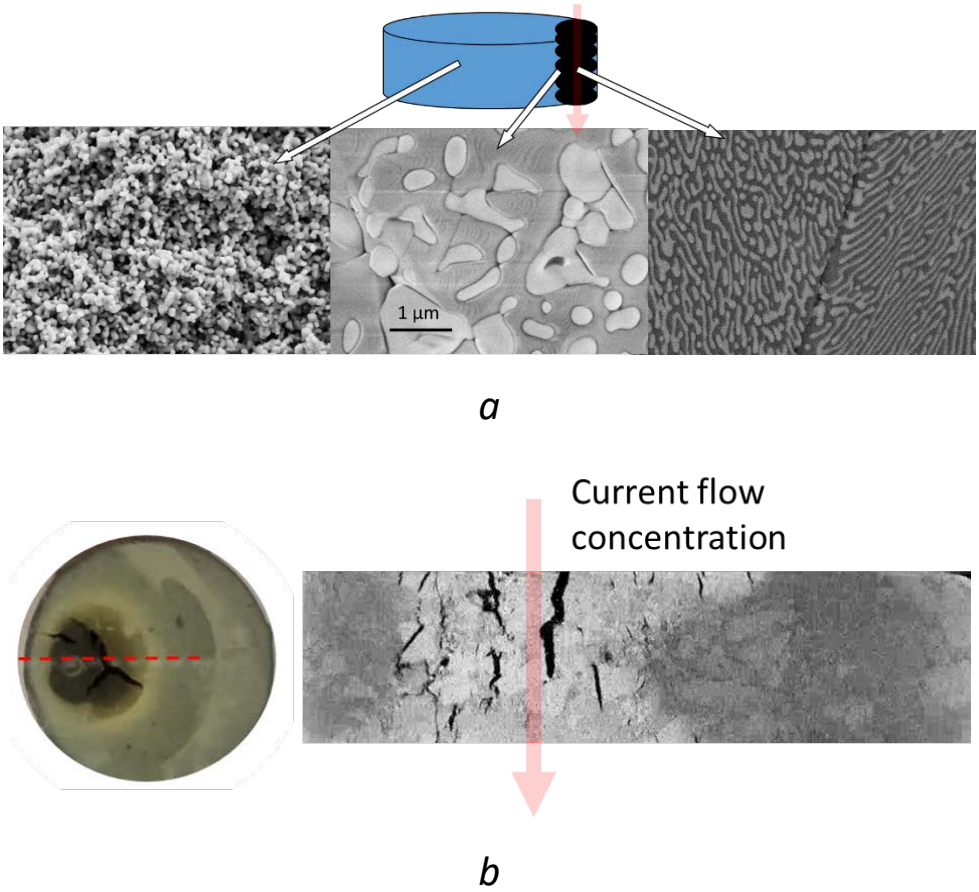

Figure 5. Current flow concentration and "hot lines" in FS experiments: mostly non densified alumina-zirconia composite pellet showing densification and grain growth and even melted eutectic along the flow axis (a)[38]; top and cross section of a LVP ($Li_3V_2(PO_4)_3$) pellet showing the localisation of densification and fracture (b).

Jerby *et al.* have studied the development of the thermal instability into a "localized microwave heating" by experiments and numerical models and qualified the phenomenon as an illustration of the "Matthew effect" [39], in reference to the Matthew apostle question "why the rich get richer and the poor get poorer?", an effect whose applications go far beyond thermal runaway [40]. In FS as well as in MWS, when the field is kept constant, the power is increasing with temperature, so that the higher the temperature, the higher the temperature increase. This does not only lead to an increase of the temperature difference (**Figure 6**-a), but also to the shrinking of the hot region as shown on normalised curves (Figure 6-b).

It can be noticed that high temperature localisation leads to locally faster densification due to sintering. As higher density means higher electrical conductivity and higher dielectric permittivity, sintering phenomena tend to enhance the localisation.

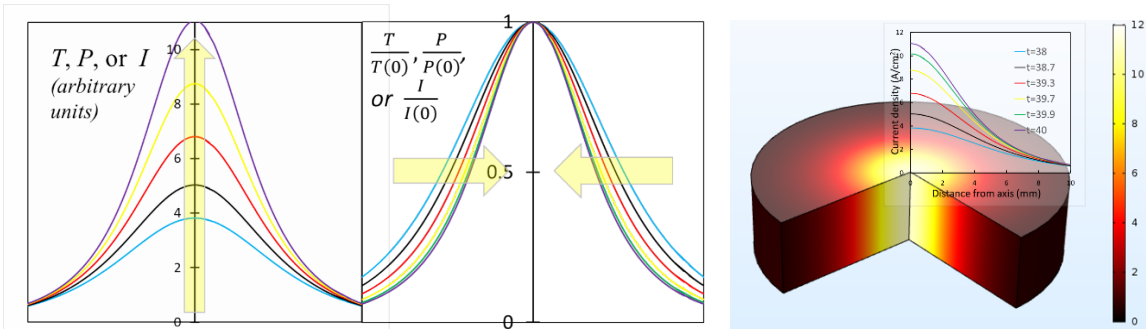

a b c

Figure 6. Initiation and development of localisation event: typical evolution of a representative physical entity (temperature T, local power P, current density I) (a) and of the normalised value showing the narrowing of the hot region (b) and numerical example of a FS cylindrical homogeneous specimen submitted to axial current and side cooling (c). The simulations presented in the present paper are performed using the electrical conductivity for YSZ proposed by Todd et al.[18], *i.e.*, $\sigma = 9302\ \exp(171\text{kJ.mol}^{-1}/\text{RT})\ \text{S/cm}^{-1}$.

Is there a limit to this temperature concentration increase? A stationary temperature profile may be reached at which the heat loss equals the electromagnetic power source. Hewitt et al. [21] have shown that in the case of FS, for a long cylindrical specimen of radius r with side heat exchange with ambient, a steady state is always expected in the fixed current situation, while in the fixed voltage configuration a steady state is only obtained when the dimensionless "strength of the ohmic heating" $\frac{E^2\sigma_0\frac{Q}{RT_0^2}}{\kappa}r^2$ (using the same notations as above) is small enough. It can be noticed that this dimensionless parameter is almost the same as the above mentioned power to loss ratio Π in Equation 10, here applied to the specimen characteristic size. This is consistent as the stability analysis and the existence of a stationary state are indeed not really different problems. Anyway, even when a steady state is mathematically expected, events such as local melting or fracture of the material may occur before the steady state is reached.

3.3. *Sources of instability nucleation*

3.3.1. Thermal exchanges

The bulk heating in both MW and FS naturally produce a thermal gradient often mentioned as "inverted gradient" with respect to the usual gradient obtained by surface heating in a classic furnace with hot walls. This inverted gradient provides an inhomogeneous temperature profile at the scale of the specimen size, suitable to trigger an instability in any large enough specimen. In the case of FS, these thermal gradients were observed in early modelling results in FS [41][42] and clearly analysed as the source of the development of instabilities in a 1D axisymmetric model [18]. Other papers only obtain limited thermal gradients in calculations, which can be related to the small thickness and width of the dog-bone shaped modelled samples [43]. In MWS, although field penetration limitations have to be taken into account in some cases, simulations clearly showed the development of such bulk hot spots [28][33][44]. Inverted gradients are a major source for nucleating centred hot spots in both FS (Figure 6-c)

and MWS. Off-centre hot spots are however frequently observed (Figure 5), revealing that other sources for nucleating hot spots may be present.

3.3.2. Field inhomogeneity

Defects in the field distribution are other sources of instability nucleation. The uncontrolled field non uniformity in multimode MW cavities (Figure 2) is one of these sources, often discussed in review papers [9][45]. The specimen is itself a source of inhomogeneity as the field distribution outside and inside results from the interaction of the microwave applied field and the specimen [28][44][46]. The field, and therefore the dissipated power depend on the specimen shape and position in the cavity and may exhibit strong inhomogeneity even at the beginning of heating (**Figure 7**).

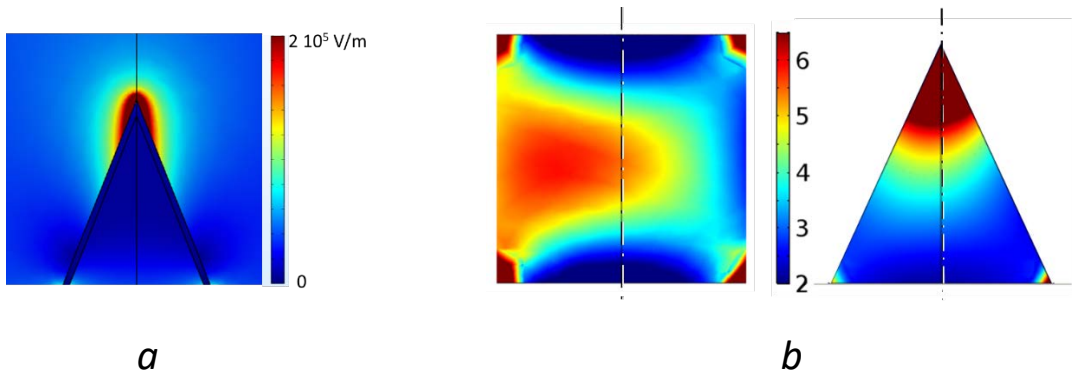

Figure 7. Examples of inhomogeneous electric field application field in MWS in a single mode cavity: field in and around an empty conical specimen (a); power density in cylindrical and conic centimetre specimens slightly off-centred from a field node (b). Simulations are performed for a 1 cm size zirconia specimen at room temperature.

In FS, the field results from the application of the voltage at contacts. When the system evolution departs from symmetry, the initial perturbation is not centred: for instance in a dog-bone shaped specimen in horizontal position hanged by the electrical wire (**Figure 8**-a), the slight off-centring is enough to induce an upward deviation from the current flow, so that the non-axially developed instability leads to a curved sample [19]. The quality of contacts is also a significant potential source of defects leading to localization (Figure 8-b): different contact configurations may lead to a variety of final defects in the FS processed parts [35].

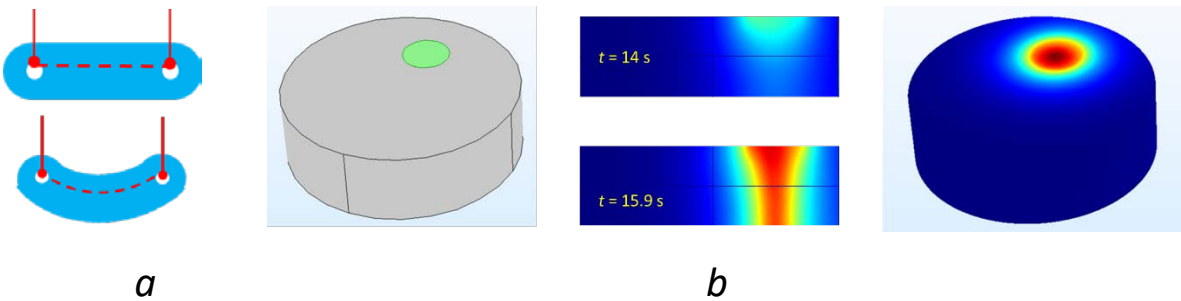

Figure 8. Examples of inhomogeneous electric field application field in FS: off-axis contacts in a dog-bone-like specimen (a); numerical simulation showing the development of the instability in a pellet with perfect bottom contact and localised top contact (b).

3.3.3. *Composition inhomogeneity*

Composition inhomogeneity is the third typical source of localisation nuclei. In MWS, the presence of particles of a highly absorbing material in a weakly coupling matrix is a cause of hot spots [47]. It must be noticed that such hot spots can in some cases be used as sintering aids ("internal susceptors") [48]. Local composition homogeneity is also mentioned to promote hot spots in other domains of microwave heating such as food defrosting [49]

In FS, local composition inhomogeneity induces preferential current paths that lead to the development of hot spots (hot lines) [50]. Even small composition variations, inducing small conductivity variations are enough to trigger preferential paths (**Figure 9**).

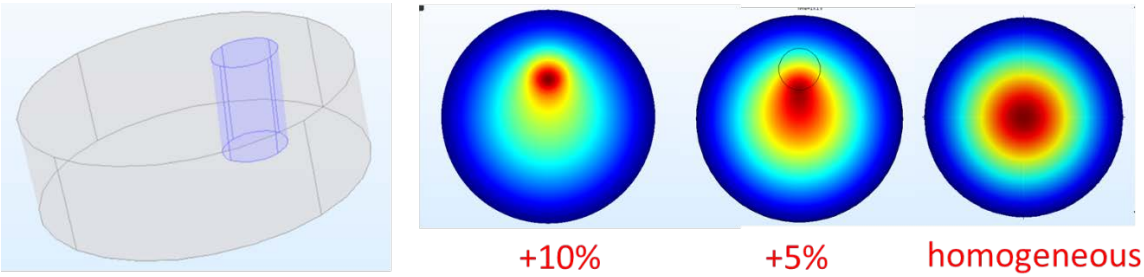

Figure 9. Example of inhomogeneous sample in FS: simulation of localisation in a zirconia specimen containing a local volume with slightly higher density, leading to 5% or 10% higher conductivity.

4. Preventing and using hot spots/localization

4.1. *Thermal and power management*

As the intrinsic instability tends to develop from any source of localisation, except for very small specimens, the first strategy consists in suppressing, limiting or compensating the sources of nucleation.

The very first idea is to reduce the thermal exchanges by using thermal insulation. It was tested with some success in the case of FS [51] using different types of insulation on small cross section (1.9X3mm^2) dog-bone shapes specimens. The second idea is to balance the natural thermal gradient by an adapted application of current. One example is the "current path management" [52] that was tested on numerical models and experiments in the case of a flat dog-bone specimen: two connections instead of one were used at each end, so that two privileged current paths, symmetric with respect to the dog-bone axis, partially balance the natural tendency for axial concentration of the current and heat production. With the same purpose of balancing the localisation tendency of current, Molina-Molina *et al.* [53] proposed to use a three-phase electrical power supply and three (or more) contacts to apply a rotating electric field ("Multi-Phase Flash Sintering") that is expected to prevent privileged current path to develop in the specimen.

In the case of MWS, thermal insulation is systematically used but it does not allow preventing localisation. For this purpose, the commonly used technique is the so-called hybrid microwave heating: parts of materials with a significant ability to couple with microwave and a weak evolution of the permittivity with temperature are placed close to or around the specimen to

be heated/sintered. They act as "susceptors" that both transform the MW energy into heat (then classically transmitted to the specimen) and limit the field applied to the specimen itself. Hybrid microwave heating appears as a good compromise [28][46], and various strategies have been developed for optimizing susceptor configurations with respect to the properties of materials to be processed [25][54].

4.2. *Process parameters management*

The second strategy is to limit or delay the development of hot spots so that high enough density is achieved before the localisation phenomena reach unacceptable levels.

Very high heating rates being conditions that promote instability, the first idea is to use a controlled heating rate, as already mentioned. This is efficient in MWS when associated to hybrid heating [27][28]. In FS, controlled current ramps used instead the usual voltage control before a 10 s current control showed efficient limitation of the current spike and favourably compared to both classic FS in the case of 3YSZ [55]. With a similar purpose, a "step-wise" technique, in which a series of progressive flashes with increasing fixed current short stages is applied, was successfully applied to sintering SOFC electrolytes [56].

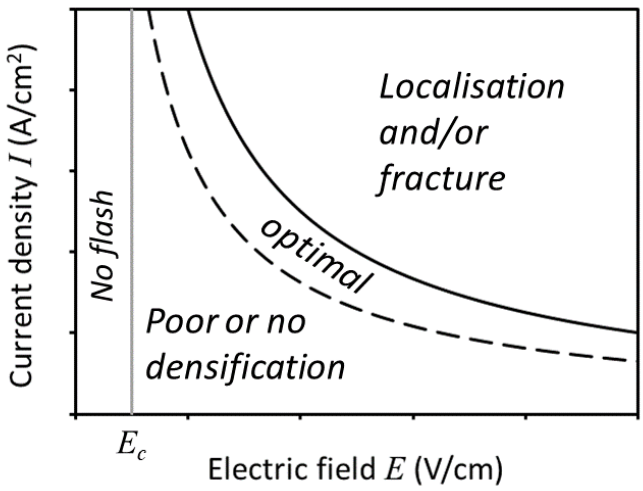

Figure 10. Schematic representation of processing map in the case of fixed temperature FS experiments with 2 steps: fixed field E then fixed current I.

In FS, the fixed current step limits the dissipated power in the specimen but does not by itself stop localisation: the power limitation may help reaching a steady state but does not guarantee it. In their experiments on $BaTiO_3$ performed by applying a constant heating rate at fixed field E M'Peko *et al.* [57] observed that current localisation occurs when the limiting current I is high. They plotted the observations in "processing maps", *i.e.*, plots of experimental results in the plane (field E, current density I). The plots showed an almost constant current density limit between "safe" and "localisation", but in these experiments the furnace temperature and electric field were strongly correlated. Several papers have reported results about such plots in the case of constant furnace temperature on different materials: 3YSZ [58], ceria [59], $BiFeO_3$ [60]. All these results are schematically summarised in **Figure 10**. As expected from previous papers no flash occurs below a critical field value E_c. Localisation is observed for high field and currents, *i.e.*, above the solid limit curve. The density of the flashed

sintered specimens is low at low values of E and increases with increasing values of E and I, leading to possible optimal processing conditions between the dashed and full curves of Figure 10. In a first order evaluation, the experimental limit should be close to constant power hyperbolas $EI = P^*$, the product EI being the maximum value of the power provided to the specimen during the FS experiment, at the transition from fixed field E to fixed current I. These processing maps are useful but only partly capture the experimental conditions, as they are drawn for a given value of the furnace temperature T_0 and a given hold time in the fixed current step, as pointed out by Trombin and Raj [58]. As previously noticed, higher furnace temperature is expected to decrease the thermal gradient that favours the hot spot formation, while increasing the hold time might favour the densification (and grain growth) as well as the development of the hot spot, so that complementary maps using the plane (current density, holding time) should also be used [6][58]. This kind of consideration was also used for developing a "continuous flash sintering" technique in which, after the flash phenomenon is initiated, a long specimen is moved at an optimal velocity between two electrodes [61].

4.3. *Using hot spots*

Hot spots and localisation phenomena can also be considered as an opportunity, when the hotspot nucleation can be controlled. Jerby *et al.* [62][63] have developed the concept of localized microwave-heating intensification and identified applications such as drilling of glass, thermite reaction ignition, or local sintering of metal powder. Riminesi & Olmi [64] proposed to use localized microwave heating against biotic agent growth within wooden artefacts and on the surface of stone artefacts.

5. Conclusion

Hot spots in FS and MWS result from the thermal runaway due the intrinsic instability of heating with an electrical or electromagnetic field when the coupling between the field and the material, *i.e.,* the heat source, increases with increasing temperature. This is the case in most ceramics. The localisation of the thermal runaway results from the competition between local heat source and local heat evacuation. It develops as the amplification of any localised temperature or electromagnetic power excess: any localisation nucleus develops when it is larger than a critical size that depends on the material and processing conditions. This amplification phenomenon is enhanced by high field and high temperature coefficient $\frac{d\gamma}{dT}$ of the coupling parameter γ (electrical conductivity σ and imaginary part of the permittivity ε_e'', respectively) and by low values of the thermal conductivity. In practice, high fields are required to get high heating rates.

A major and systematic source from which the localisation develops is the inverted temperature gradient of the part inherent to these heating techniques. Any default of the specimen or the process conditions with local character can also initiate the phenomenon: local composition or field variations, inhomogeneous electrical contact can be the practical source of hot spots.

Two types of approaches have been proposed in the literature to prevent or limit hot spots. The first one consists in limiting the nucleation, *e.g*. by trying to suppress thermal gradients or by using geometries and field applicators that are expected to balance the thermal gradients. The second approach is illustrated by the “processing maps”, that aim at identifying process conditions in which optimal results can be obtained. These maps evidence the compromises to be found between the target properties (density, homogeneity) and the process parameters.

Although localisation is almost unavoidable, both types of approaches contribute to obtain acceptable conditions for the densification of homogeneous ceramic parts while keeping the expected advantages of field assisted techniques, namely fastness and energy saving.

Acknowledgements

This work was supported by the French National Research Agency through ANR-17 CE08 0021 and ANR-20-CE05-0040-02 projects and by the Centre of Excellence of Multifunctional Architectured Materials “CEMAM”.

References

[1] D.E. Clark, W.H. Sutton, *Annu Rev Mater Sci* **1996**, 299.
[2] S. Chandrasekaran, S. Ramanathan, T. Basak, *AIChE J.* **2012**, *58*, 330.
[3] J.-M. Chaix, in *Ref. Module Mater. Sci. Mater. Eng.*, Elsevier**2020**, B9780128185421000000.
[4] C.E.J. Dancer, *Mater. Res. Express* **2016**, *3*, 102001.
[5] M. Yu, S. Grasso, R. Mckinnon, T. Saunders, M.J. Reece, *Adv. Appl. Ceram.* **2017**, *116*, 24.
[6] M. Biesuz, V.M. Sglavo, *J. Eur. Ceram. Soc.* **2019**, *39*, 115.
[7] S.K. Jha, R. Raj, *J. Am. Ceram. Soc.* **2014**, *97*, 527.
[8] O. Guillon, R.A. De Souza, T.P. Mishra, W. Rheinheimer, *MRS Bull.* **2021**, *46*, 52.
[9] M.A. Janney, C.L. Calhoun, H.D. Kimrey, *J. Am. Ceram. Soc.* **1992**, *75*, 341.
[10] R. Wroe, A.T. Rowley, *J. Mater. Sci.* **1996**, *31*, 2019.
[11] K.H. Brosnan, G.L. Messing, D.K. Agrawal, *J. Am. Ceram. Soc.* **2003**, *86*, 1307.
[12] K.I. Rybakov, E.A. Olevsky, V.E. Semenov, *Scr. Mater.* **2012**, *66*, 1049.
[13] W. Ji, B. Parker, S. Falco, J.Y. Zhang, Z.Y. Fu, R.I. Todd, *J. Eur. Ceram. Soc.* **2017**, *37*, 2547.
[14] G. Xu, I.K. Lloyd, Y. Carmel, T. Olorunyolemi, O.C. Wilson, *J. Mater. Res.* **2001**, *16*, 2850.
[15] M. Cologna, B. Rashkova, R. Raj, *J. Am. Ceram. Soc.* **2010**, *93*, 3556.
[16] J.S.C. Francis, *Small Flash Movie* **2012**, *https://www.youtube.com/watch?v=HvOfoyhu2aE*.
[17] K.S. Naik, V.M. Sglavo, R. Raj, *J. Eur. Ceram. Soc.* **2014**, *34*, 4063.
[18] R.I. Todd, E. Zapata-Solvas, R.S. Bonilla, T. Sneddon, P.R. Wilshaw, *J. Eur. Ceram. Soc.* **2015**, *35*, 1865.
[19] M. Yoshida, S. Falco, R.I. Todd, *J. Ceram. Soc. Jpn.* **2018**, *126*, 579.
[20] Y. Dong, I. -Wei Chen, *J. Am. Ceram. Soc.* **2015**, *98*, 3624.
[21] I.J. Hewitt, A.A. Lacey, R.I. Todd, *Math. Model. Nat. Phenom.* **2015**, *10*, 77.
[22] Y. Dong, I. -Wei Chen, *J. Am. Ceram. Soc.* **2015**, *98*, 2333.
[23] J.G.P. da Silva, H.A. Al-Qureshi, F. Keil, R. Janssen, *J. Eur. Ceram. Soc.* **2016**, *36*, 1261.
[24] E. Bichaud, J.M. Chaix, C. Carry, M. Kleitz, M.C. Steil, *J. Eur. Ceram. Soc.* **2015**, *35*, 2587.
[25] C.E. Holcombe, N.L. Dykes, *J. Mater. Sci. Lett.* **1990**, *9*, 425.
[26] J. Croquesel, D. Bouvard, J.-M. Chaix, C.P. Carry, S. Saunier, *Mater. Des.* **2015**, *88*, 98.
[27] S. Marinel, N. Renaut, E. Savary, R. Macaigne, G. Riquet, C. Coureau, T. Gadeyne, D. Guillet, *Adv. Mater. Sci. Eng.* **2018**, *2018*, 1.
[28] T. Garnault, D. Bouvard, J.-M. Chaix, S. Marinel, C. Harnois, *Ceram. Int.* **2021**, S0272884221006210.
[29] G. Roussy, A. Bennani, J.-M. Thiebaut, *J. Appl. Phys.* **1987**, *62*, 1167.
[30] M.S. Spotz, D.J. Skamser, D.L. Johnson, *J. Am. Ceram. Soc.* **1995**, *78*, 1041.
[31] Y. Bykov, S. Egorov, A. Eremeev, V. Kholoptsev, I. Plotnikov, K. Rybakov, A. Sorokin, *Materials* **2016**, *9*, 684.
[32] Y. Dong, *ArXiv Prepr.* **2017**, arXiv:1702.05565.
[33] C. Manière, T. Zahrah, E.A. Olevsky, *Scr. Mater.* **2017**, *128*, 49.

[34] Garnault, *Frittage Par Micro-Ondes de Céramiques Mises En Forme Par Impression 3D*, Université Grenoble Alpes, **2020**.
[35] M.Z. Becker, S. Baltianski, L. Popilevsky, R. Attias, T. Paul, Y. Tsur, *Adv. Eng. Mater.* **2021**, *23*, 2001499.
[36] H. Zhou, X. Li, Y. Zhu, J. Liu, A. Wu, G. Ma, X. Wang, Z. Jia, L. Wang, *High Volt.* **2021**, hve2.12080.
[37] M.C. Steil, D. Marinha, Y. Aman, J.R.C. Gomes, M. Kleitz, *J. Eur. Ceram. Soc.* **2013**, *33*, 2093.
[38] E. Bichaud, *Frittage « flash » de Céramiques Sous Courant Alternatif*, Université Grenoble Alpes, **2016**.
[39] E. Jerby, *AMPERE Newsl.* **2019**, 1.
[40] R.K. Merton, *Science* **1968**, *159*, 56.
[41] S. Grasso, Y. Sakka, N. Rendtorff, C. Hu, G. Maizza, H. Borodianska, O. Vasylkiv, *J. Ceram. Soc. Jpn.* **2011**, *119*, 144.
[42] J.G. Pereira da Silva, J. Lebrun, H.A. Al-Qureshi, R. Janssen, R. Raj, *J. Am. Ceram. Soc.* **2015**, *98*, 3525.
[43] A. Eqbal, K.S. Arya, T. Chakrabarti, *Ceram. Int.* **2020**, *46*, 10370.
[44] C. Manière, F. Borie, S. Marinel, *J. Manuf. Process.* **2020**, *56*, 147.
[45] R.R. Mishra, A.K. Sharma, *Compos. Part A* **2016**, *81*, 78.
[46] C. Manière, T. Zahrah, E.A. Olevsky, *J. Am. Ceram. Soc.* **2017**, *100*, 2439.
[47] W. Wang, B. Wang, J. Sun, Y. Mao, X. Zhao, Z. Song, *RSC Adv.* **2016**, *6*, 52974.
[48] S. Fan, H. Zheng, Q. Gao, Y. Li, Y. Chen, G. Liu, B. Fan, R. Zhang, *Int. J. Appl. Ceram. Technol.* **2020**, *17*, 2250.
[49] J.C. Atuonwu, S.A. Tassou, *J. Food Eng.* **2018**, *234*, 1.
[50] Y. Cao, G.-C. Xu, F. Smeacetto, P. Shen, *Open Ceram.* **2022**, *12*, 100301.
[51] M. Biesuz, J. Dong, S. Fu, Y. Liu, H. Zhang, D. Zhu, C. Hu, S. Grasso, *Scr. Mater.* **2019**, *162*, 99.
[52] Y. Li, R. Torchio, S. Falco, P. Alotto, Z. Huang, R.I. Todd, *J. Eur. Ceram. Soc.* **2021**, *41*, 6649.
[53] S. Molina-Molina, E. Gil-González, F.J. Durán-Olivencia, J.M. Valverde, A. Perejón, P.E. Sánchez-Jiménez, L.A. Pérez-Maqueda, *Appl. Mater. Today* **2022**, *26*, 101274.
[54] M. Bhattacharya, T. Basak, *Energy* **2016**, *97*, 306.
[55] K.H. Christian, H. Charalambous, S.K. Jha, T. Tsakalakos, *J. Eur. Ceram. Soc.* **2020**, *40*, 436.
[56] J. Zhang, Y. Zhao, J. Qiao, W. Sun, K. Sun, Z. Wang, *Int. J. Hydrog. Energy* **2020**, *45*, 17824.
[57] J.-C. M'Peko, John.S.C. Francis, R. Raj, *J. Eur. Ceram. Soc.* **2014**, *34*, 3655.
[58] F. Trombin, R. Raj, *Am. Ceram. Soc. Bull.* **2014**, *93*, 32.
[59] T.P. Mishra, C. Lenser, R. Raj, O. Guillon, M. Bram, *J. Am. Ceram. Soc.* **2021**, *104*, 4316.
[60] E. Gil-González, A. Perejón, P.E. Sánchez-Jiménez, D. Román-González, L.A. Pérez-Maqueda, *Ceram. Int.* **2020**, *46*, 29413.
[61] E. Sortino, J. Lebrun, A. Sansone, R. Raj, *J. Am. Ceram. Soc.* **2018**, *101*, 1432.
[62] E. Jerby, *Chem. Eng. Process. Process Intensif.* **2017**, *122*, 331.
[63] Y. Meir, E. Jerby, in *Proc. 2nd Glob. Congr. Microw. Energy Appl.*, Long Beach, CA,USA **2012**, 131.
[64] C. Riminesi, R. Olmi, *Int. J. Conserv. Sci.* **2016**, *7*, 281.